

Synthesis, Applications, and Prospects of Quantum-Dot-in-Perovskite Solids

Haijie Chen, Joao M. Pina, Yi Hou, and Edward H. Sargent*

Quantum-dot-in-perovskite solids (QDiP), wherein colloidal quantum dots (CQDs) are inside bulk hybrid halide perovskites, have emerged as a novel class of semiconductors with mixed dimensionalities. The interfacial quality achieved enables good charge transport from the perovskite matrix to the embedded dots and leads to photon interaction functionalities that go beyond those of the single-phase constituents. In this review, recent advances in the synthesis and compositions of QDiP are showcased, the improved optoelectronic properties are discussed, and their applications are explored. The authors focus on how the combination of CQDs and halide perovskites enhances stability, charge transport, and carrier diffusion length. Progress in device operation (prominently, light-emitting diodes and solar cells) is summarized, and a perspective on future opportunities for QDiPs is given.

that of more conventional bulk semiconductors.^[10–16] Halide perovskites, another promising optoelectronic material family, have attracted extensive interest during the past decades because of their high carrier mobility, long carrier lifetime, and high defect tolerance.^[17–20]

Halide perovskites and quantum-tuned CQDs have been combined to form quantum-dot-in-perovskite solids (QDiP).^[2] This leverages the judicious selection of the perovskite semiconductors and the semiconductor constituents of the CQDs with lattice match in mind. QDiP have opened new directions in otherwise well-studied CQDs and halide perovskites.

Since the first report of QDiP using PbS-CH₃NH₃PbI₃ (MAI) in 2015,^[2] this concept has drawn increasing attention, and extensive progress has been achieved. With the design and selection of suitable CQDs and halide perovskites, several new QDiP systems have been synthesized and applied in optoelectronic devices. Moreover, perovskites capped with CQDs have also been synthesized.^[21,22] Core/shell structured perovskite/CQDs, for example, growing CsPbI₃ NCs in a solution with ultrasmall PbS CQDs available, were successfully applied to optoelectronic devices.^[21]

This review highlights the achievements obtained with QDiP and identifies future development opportunities. Several excellent reviews related to QDiP have been published.^[23–25] We focus on the QDiP materials themselves, first introducing synthesis techniques, and then discussing the interface engineering between the CQDs and halide perovskites. We then discuss the properties that emerge when combining both, and finish with a discussion of QDiP applied to optoelectronic devices.

1. Introduction


Heteroepitaxy, the growth of a crystal onto the surface of another, enables the design and realization of functions that are not attainable with the single-phase constituents.^[1,2] The concept has been applied to 2D superconductivity such as in Bi₂Se₃/FeTe heterostructures;^[3] featured in emerging quantum phenomena in WSe₂-WS₂ and MoSe₂-WSe₂ superlattices;^[4,5] and integrated into metal-organic frameworks (MOFs) and polymer hybrid materials used in gas separation, sensing, catalysis, and storage.^[6,7]

Colloidal quantum dots (CQDs), which are nanoscale crystals of the corresponding bulk semiconductors, combine high photoluminescence efficiency, narrow emission linewidth, and size-tuned optoelectronic properties, with the low-cost associated with solution-processability.^[8,9] They are used in optoelectronic devices, such as photodetectors, light-emitting devices, and solar cells, achieving equal or superior performance as

Dr. H. Chen, J. M. Pina, Prof. Y. Hou, Prof. E. H. Sargent
The Edward S. Rogers Department of Electrical and Computer
Engineering

University of Toronto
Toronto, Ontario M5S 3G4, Canada
E-mail: ted.sargent@utoronto.ca

Dr. H. Chen
State Key Laboratory for Modification of Chemical
Fibers and Polymer Materials
Institute of Functional Materials
College of Materials Science and Engineering
Donghua University
Shanghai 201620, China

 The ORCID identification number(s) for the author(s) of this article can be found under <https://doi.org/10.1002/aenm.202100774>.

DOI: 10.1002/aenm.202100774

2. Synthesis and Interface Engineering of QDiP

Conventional CQDs, such as PbS, PbSe, PbTe, CdSe, and ZnS, are typically binary semiconductors.^[26–30] The sizes of the nanocrystals are usually of 2–20 nm to retain quantum confinement effects.^[31] By controlling the size, exposed facets, and surface ligands, one can design promising electronic and optical properties. For halide perovskite semiconductors (APbX₃), the bandedge arises from the X and Pb atoms: the valence band (VB) and conduction band (CB) are formed via the hybridization of Pb 6s and halide p-orbitals. The antibonding states contribute to both VB and CB, while halide orbitals to the CB. The electronic structure of the perovskite is tuned by changing

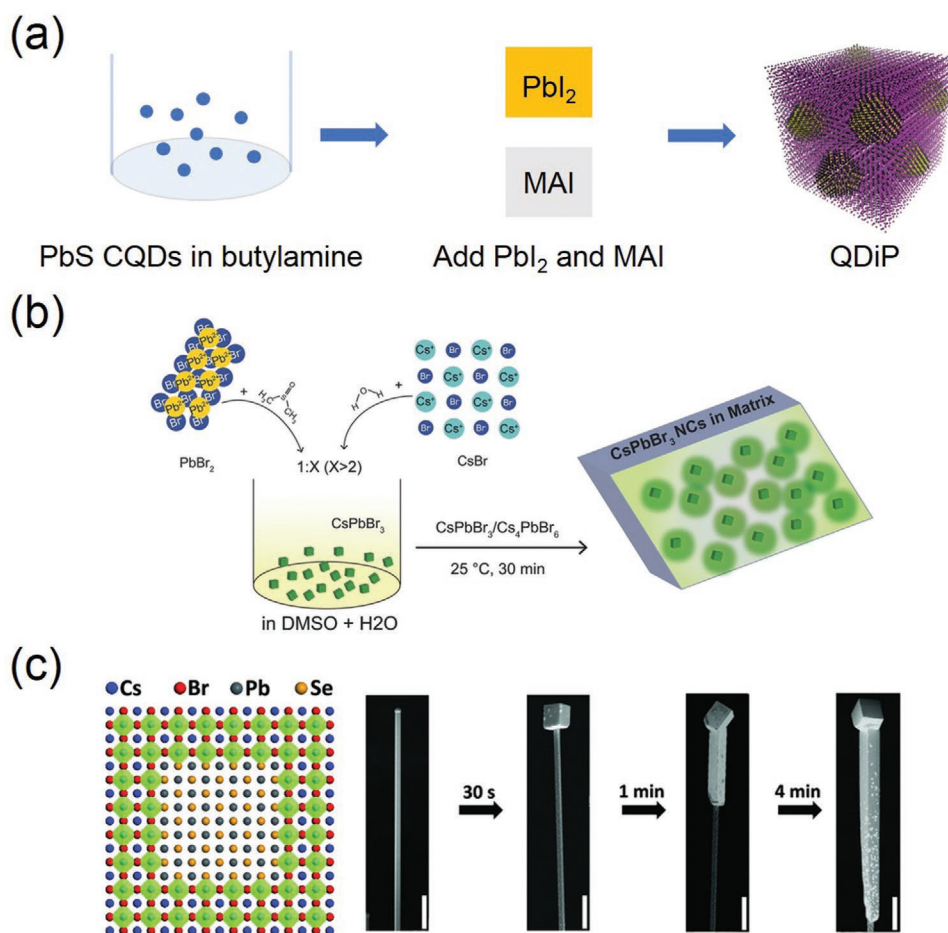


Figure 1. a) Two-step synthesis of QDiP. Reproduced with permission.^[2] Copyright 2015, Springer Nature. b) Synthesis of CsPbBr₃-in-Cs₄PbBr₆ solids. Reproduced with permission.^[35] Copyright 2017, Wiley. c) Schematic cross-section showing the atomic arrangement for PbSe-CsPbBr₃ core-shell wire and the SEM images of the representative heterostructure with different growth times. Reproduced with permission.^[36] Copyright 2018, Wiley.

the halide elements. Although the A site does not contribute directly to the bandstructure, the abundance of options for organic candidates has led to diverse materials in the perovskite family. These 3D perovskites can be tuned into 2D, 1D and 0D compounds, offering additional semiconducting hybrids.^[32–34]

2.1. Synthesis Approaches

Both CQDs and halide perovskites are solution-processable, enabling simultaneous solvation for ensuing chemical reactions. The majority of QDiP reports use a two-step approach to assemble CQDs within a perovskite matrix. For the synthesis of PbS-MAPbI₃ QDiP (Figure 1), CQDs are prepared in advance using an established hot injection method. The original oleic acid (OA) ligands of the CQDs are then exchanged with lead iodide and MAI and re-dispersed in butylamine.^[2] A stoichiometric amount of perovskite precursors (PbI₂ and MAI) is then co-dispersed in the CQD in butylamine solution before film fabrication through spin-coating^[37–39] Iodide ligand exchange was conducted by mixing the CQD in octane with a solution containing MAPbI₃ perovskite precursors. A similar methodology was also successfully used for SnS-MAPbI₃ QDiP.^[40] As an alternative to dispersing CQDs and perovskite precursors

together, one may disperse the CQDs in the antisolvent used to trigger perovskite formation through spin-coating.^[41]

Heteroepitaxy of crystalline materials with different elemental compositions is often hindered by large lattice mismatches. This limits the set of material systems that can be synthesized and applied to optoelectronic devices. However, heteroepitaxy can also be implemented using materials with similar elemental composition but with different crystal structures, leading to intriguing bi-phase material systems.^[42] Following this approach, QDiP of CsPbBr₃-Cs₄PbBr₆ (Figure 1b) with improved passivation and high photoluminescent efficiency were synthesized.^[35] The ternary phase diagram of Cs, Br, and Pb shows that the cubic CsPbBr₃ phase falls onto the same line of equilibrium with rhombic Cs₄PbBr₆. By controlling the stoichiometry of the precursor solutions, QDiP are obtained by slowly injecting CsBr in water into a solution PbBr₂ in dimethylsulfoxide. Due to the poor solubility of PbBr₂ in water, precipitates are formed and can be further deposited onto a substrate by spin-coating. The cubic CsPbBr₃ nanocrystals are well incorporated into air-stable rhombic Cs₄PbBr₆ solids. Unfortunately, this is limited to the Cs-Pb-Br system, and does not appear to be strategy generalizable across most or all QDiP.

As shown in Figure 1c, a one-step chemical vapor deposition (CVD) has also been deployed to grow PbSe-CsPbBr₃

heterostructures.^[36] The perovskite can be grown onto PbSe due to the cubic crystal structure and the small lattice mismatch of 4.8%. Pre-grown PbSe nanowires are placed in a CVD chamber where a stoichiometric mixture of PbBr₂ and CsBr is evaporated within a nitrogen environment. The Pb particles provide nucleation sites for the growth of CsPbBr₃ crystals, which happens directionally from the tip to the bottom of the PbSe wire. The successful growth of PbSe-CsPbBr₃ wires indicates that a PbSe-CsPbBr₃ QDiP may be obtained by CVD techniques based on PbSe CQDs, a concept potentially extensible to other QDiP.

2.2. Interface Engineering

On the one hand, the surface of CQDs triggers perovskite nucleation and seeds the crystal growth. On the other hand, the perovskite acts as a protection layer to militate against CQD aggregation. The surface of CQD triggers fast perovskite nucleation, likely a result of the interaction with Pb dangling bonds, enabling the incorporation of CQDs into the matrix. MA⁺/FA⁺ have been successfully used as short ligands to exchange for the original large-chain organic molecules on CQD surfaces. In one study,^[43] PbS nanoparticles were capped with oleic acid (OA), a long alkyl chain that does not enable dispersion in dimethylformamide. OA ligands were therefore exchanged for halides, enabling CQD dispersion in a polar solvent to permit integration with perovskites. The interface between CQDs and halide perovskites plays a fundamental role in the carrier transport dynamics further affecting the optical and electrical properties of the material system.

As a result of diverse values of bandgaps and different band positions, the interface between CQDs and halide perovskites exhibits a discontinuous step in both the CB and VB. As shown in **Figure 2**, offsets can lead to type-I (straddling gap), type-II (staggered gap), and type-III (broken gap).^[23] For type-I band alignment, CQDs with wide-bandgap halide perovskites will confine excitons to their core, leading to enhanced photoluminescence. This enables type-I QDiP as emitting layers in light-emitting diodes (LED), for example, PbS-PEACs_{n-1}Pb_nBr_{3n+1}.^[44] For type-II, the excited electrons will transfer to the perovskite

matrix (with lower CB edges) and holes to the core CQDs (with higher VB edge). The opposite type-II alignment, with excited electrons transferring to the CQDs and holes to the perovskite, can also be achieved. This charge separation is of interest when long-lived excited states are desired, such as in solar cells and photodetectors, for example, CuInSe₂-MAPbI₃.^[41] The position of the bands is determined by the individual constituents: in fact, the bandstructure at the interface may be controlled by modifying the surface of the CQDs, the bonding between CQDs and lead ions, and grain defects. The measurement of true band positions in QDiP, specifically at the CQD-perovskite interface, is a topic that will benefit from further investigation.

3. Properties of QDiP

3.1. Optical Properties

The optical properties of QDiP relate to the properties of the constituent CQDs, perovskites, and their interface. For the PbS-MAPbBr₃ QDiP, upon CQD loading, there is no change in the X-ray diffraction pattern of the perovskite (**Figure 3a**). The perovskite matrix remains unaltered in the new material.^[45] Simultaneously, MAPbBr₃ and PbS peaks are observed in the absorption spectra (**Figure 3b**). In all, the results demonstrate that CQD and perovskite constituents contribute to the properties of the integrated QDiP, and each remains intact in the final solid. The PL intensity of MAPbBr₃ decreases when more CQDs are loaded (**Figure 3c**), demonstrating efficient charge transfer through the interface of MAPbBr₃ and PbS. Other QDiP material systems with type-I heterojunction equally have decreased perovskite photoluminescence in return for improved CQD photoluminescence.^[47]

3.2. Stability

A challenging issue for halide perovskites is their limited stability in ambient conditions, which hinders practical applications. CQDs come with challenges of their own: they are

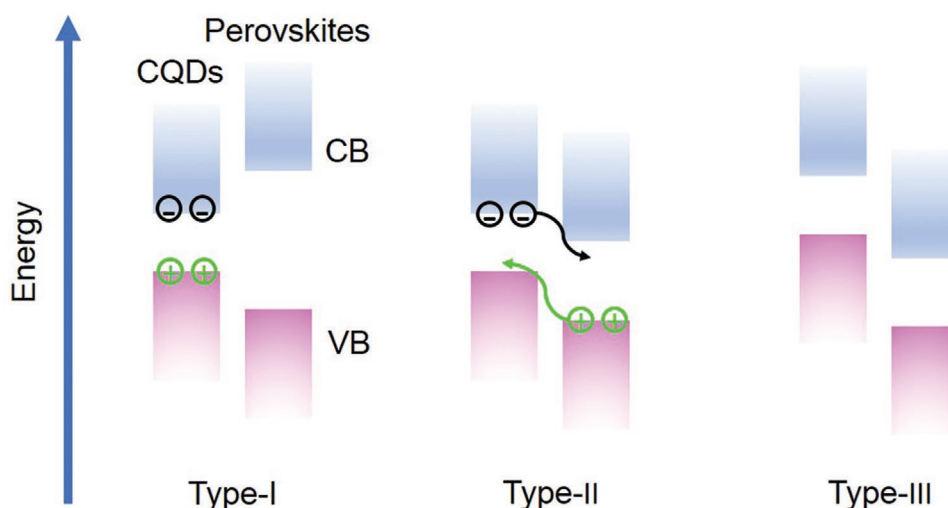


Figure 2. Different band alignments in QDiP, which depend on the bandgap and band positions of the CQDs and perovskites.

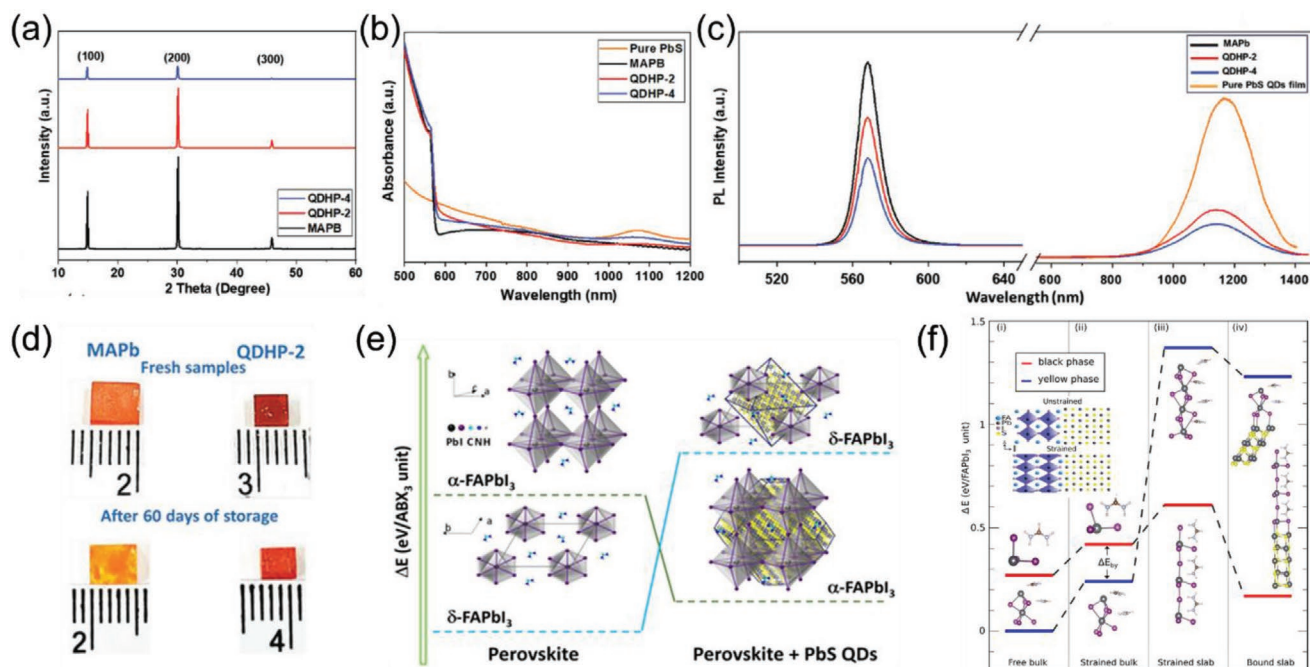


Figure 3. a) X-ray diffraction patterns, b) optical absorption, and c) photoluminescence spectra of MAPbBr₃ and PbS-MAPbBr₃ QDiP. Reproduced with permission.^[45] Copyright 2020, Wiley. d) Optical images of MAPbBr₃ and QDiP single crystals (up panel) freshly prepared and (down panel) stored in ambient for 60 days. Reproduced with permission.^[45] Copyright 2020, Wiley. e) The PbS CQD in FAPbI₃ matrix favors the black phase rather than the yellow. Reproduced with permission.^[46] Copyright 2020, ACS. f) Total energy DFT calculation of i) black and yellow bulk FAPbI₃ phases represented by red and blue colors, respectively, ii) the effect of strain on the bulk when matching the PbS lattice, iii) the presence of surfaces in the slabs, and iv) the role of chemical binding to the PbS substrate in the QDiP. The inset shows a comparison between the unstrained and strained structures. Reproduced with permission.^[46] Copyright 2020, ACS.

prone to aggregation and surface oxidation. In principle, the perovskite matrix could militate desirably these processes against each other. To study the impact of CQD additives on the stability of perovskites, Younis et al. grew perovskite-only and QDiP single crystals to find that the stability was greatly improved in the presence of CQDs.^[45] The surface of perovskite-only crystals (MAPbI₃) became yellow after air exposure, while QDiP single crystals (Figure 3d) did not degrade within a time frame of 2 months.

The inclusion of CQDs not only plays a role in the crystallization of perovskite but can also help to stabilize the perovskite phase. FAPbI₃ has black (cubic (α), tetragonal (β and γ)) and yellow hexagonal (δ) phases (Figure 3e). The black phase is typically unstable, yet, is desired for its suitable bandgap for solar-cell applications. In PbS-FAPbI₃ QDiP, the CQD-perovskite interface stabilizes the black phase in ambient conditions.^[46] The black phase is favored over the yellow phase because of the strong interfacial bonds formed during the epitaxial growth. The phase transition from black to yellow CsPbI₃ is also hindered by the epitaxial alignment between CsPbI₃ and CQDs.^[47] Samples remain stable for more than 6 months in ambient conditions. Other strategies to hinder the formation of the undesired yellow phase of FAPbX₃ or CsPbX₃ are cation or anion alloying.^[48–51] Alloying changes the bandstructure of the perovskite, making it less suitable for solar-cell applications. In contrast, PbS CQDs embedded into a perovskite matrix improve the stability of the material system while retaining the desired bandstructure.

To explore the reasons underpinning CQD stabilization, Masi et al. carried out first-principles calculations to uncover the role

of strain, surface planes, and chemical binding of CQDs to the perovskite matrix.^[46] Strain is present in the CQD-perovskite interface due to lattice mismatch (Figure 3f). Strain is mostly felt within the FAPbI₃ since the perovskite has a softer structure than PbS CQDs,^[52] leading to long-range tetragonal distortions of the FAPbI₃ lattice (panel (ii) of Figure 3f). This process suppresses further the formation of the yellow phase in favor of the black perovskite phase.

The surface of PbS CQDs is majorly composed of (111) crystal planes. The lattice constant of the CQDs matches well with the (100) planes of the black phase of FAPbI₃, but it has a mismatch with the preferred (111) planes of the yellow perovskite phase. This arrangement increases the formation energy of the yellow perovskite phase, making the black perovskite phase more prone to form (panel (iii) of Figure 3f).

The chemical binding of FAPbI₃ to PbS is illustrated in panel (iv) of Figure 3f. The chemical binding for both the yellow and black phases reduces the formation energy in comparison to perovskite-only crystals; however, the energy is decreased more pronouncedly for the black perovskite phase.

These factors combine to stabilize the black phase of FAPbI₃ and CsPbI₃.

3.3. Charge Transport

Compared with the CQD-only system, the addition of the halide perovskite matrix provides superior channels for carrier injection into the embedded CQDs, or for fast extraction of

carriers from the CQDs into the matrix, depending on the heterostructure type.^[45] To explore the effect of the matrix in QDiP, Z. J. Ning et al. embedded CQDs into a NaI matrix and into a perovskite for comparison.^[2] The photoluminescence quantum efficiency (PLQE) of CQDs in the NaI is about half of that of CQDs in the MAPbI₃ matrix (≈9%), which can be assigned to the high electron mobility of MAPbI₃. CQDs in NaI matrix exhibit a fivefold increase in carrier lifetime compared with only-CQDs samples. This confirms that band-tuning of the QDiP is an efficient way of improving the charge transport properties of CQDs.

To study charge transport in QDiP as a function of CQD concentration in the perovskite, M. X. Liu et al. prepared QDiP with low versus high CQD loading.^[47] **Figure 4** depicts charge transport in different samples. At low CQD loading, the carriers in the perovskite matrix transfer efficiently to the core CQDs; while at high loading, charge transfer among CQDs is achieved. It is found that the efficiency of the carrier transfer is over 87% at high CQD loading, in agreement with complete photoluminescence quenching arising from the perovskite matrix. The authors also investigated the PLQE of films having different matrix compositions to explore the effect of strain. With increasing bromine doping (up to 67% concentration), the PLQE of CQDs increases, and reaches a maximum value at ≈30%. In this composite, the lowest lattice mismatch is achieved, that is, minimal strain is preferred for higher photoluminescence.

4. Applications of QDiP

4.1. LED

CQDs have been used in LEDs because of size-tunable luminescence, narrow emission linewidth, high PLQE, compatibility with solution processing, and good photostability.^[14,53] CQD-based LEDs have shown acceptable performances both in the visible and the near-infrared (NIR) spectral regions.^[54] However, shell-free CQDs exhibit low PLQE due to unpassivated surface traps. The core-shell approach passivates the surface traps and provides localization of the electron-hole pair relative to the host and relative to neighbors, leading to an improvement in PLQE. Insulating organic ligands^[8] and polymer matrix^[55] strat-

egies were adopted to address this problem, but devices require high power consumption (high voltage) to inject sufficient current to offer bright light emission.

With QDiP, such as PbS-MAPbI₃Br_{1-x}, X. W. Gong et al. report a NIR LED with an external quantum efficiency (EQE) of 4.9%, an improvement relative to prior CQD NIR devices.^[53] For comparison, the EQE value is ≈0.03% for CQD-only control devices. The electron-hole pairs were delivered to the CQDs via the perovskite matrix. By tuning the bromine-iodine ratio of the perovskite mixture, the strain was optimized, and defects were limited both in the perovskite and at the interface with CQDs.

A mixture of CQDs in the more stable low-dimensional perovskite matrix was then adopted to increase further the efficiency of NIR LED.^[44] The utilization of low-dimensional perovskites provides controllable excitonic energy transfer into the CQDs, avoiding thereby non-radiative Auger recombination. LEDs showed an EQE of 8.1% and radiance of 7.4 W Sr⁻¹ m⁻² in the NIR, with tunable emission from 986 to 1564 nm. The devices also showed increased operating stability compared to prior generations of QDiP devices.^[53] These operated for over 1 h at a continuous current density of 10 mA cm⁻². Similar trends were seen in related CsPbBr₃ studies.^[56]

M. Vasilopoulou et al. reported a new approach to improve further the stability of QDiP. Using silica-encapsulated silver sulfide (Ag₂S@SiO₂) CQDs dispersed in a cesium-containing triple cation perovskite, they generated an emissive layer with 84% PLQE, in which the electron and hole injection were well balanced. LED emission was thereby extended to the biological NIR window (1000–1700 nm) with an EQE of 17% at a peak emission wavelength of ≈1400 nm.^[57]

4.2. Solar Cells

Both CQDs and perovskites have been widely applied in solar cells. CQDs bring the benefit of offering to harvest the infrared portion of the solar spectrum, potentially enabling multijunction solar cells.^[58] Etgar et al. used PbS CQDs embedded in perovskites to modify the absorption of MAPbI₃ (limited to 1.57 eV) for full light absorption in solar cells.^[59] The power conversion efficiency (PCE) was improved from 3.0% to 3.6% with the addition of PbS CQDs.

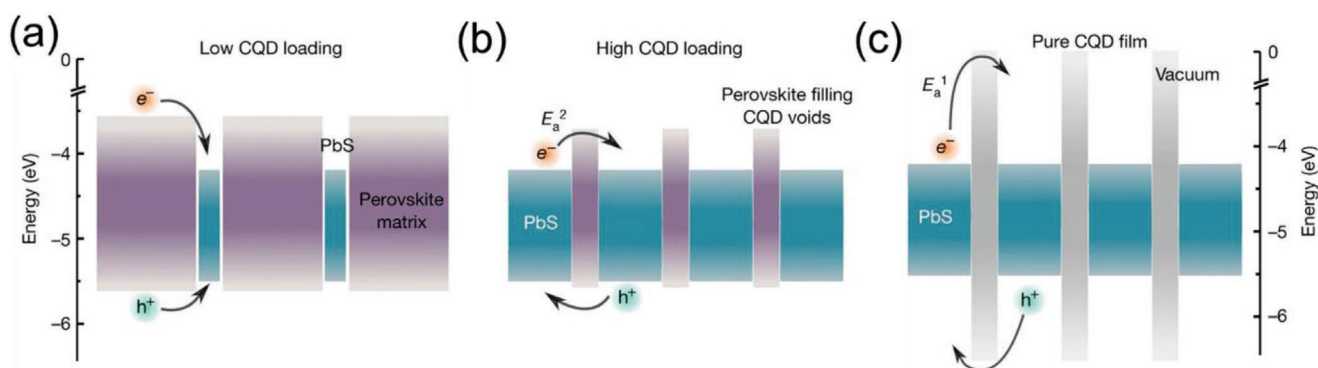


Figure 4. Schematic illustrating charge transport in samples with a) low CQD loading, b) high CQD loading, and c) only CQDs. Reproduced with permission.^[47] Copyright 2019, Springer Nature.

By improving the assembly of CQDs with the aid of perovskites, Z. Y. Yang et al. utilized PbS-MAPbI₃ QDiP and optimized PCE to 9% with fill factor (FF) of ≈68%.^[39] This work reported a depletion width of 120 nm in QDiP based devices. X. L. Zhang et al. confirmed the wide depletion region in PbS-CsPbI₃ QDiP based solar cells.^[60] They further pointed out that the superior photovoltaic performance in QDiP solar cells can be attributed to a combination of the wider depletion region, high built-in potential, and low trap density in the CQD solid, enhancing charge collection, improving carrier lifetime, and reducing bulk recombination. J. J. Peng et al. used MAPbI₃ capped PbS CQDs for solar cells achieving a PCE of 4.25% with an impressive photocurrent density (J_{sc}) of 24.83 mA cm⁻² and a relatively low FF of 38%.^[61] With all inorganic PbS-CsPbBr₂I QDiP, M. X. Liu et al. obtained PCE 12.6% with FF of 68% and superior photostability, retaining 95% of the initial PCE following 2 h continuous illumination.^[47]

In addition to the well-known PbS CQDs, black phosphorus CQDs (BPQDs) have emerged in solar applications in light of a high absorption coefficient, high electron mobility (≈1000 cm² V⁻¹ s⁻¹), and the potential of self-repair.^[62,63] BPQDs were incorporated into organic-inorganic hybrid halide perovskites^[64–66] where black phosphorus was similarly found to play a role in perovskite nucleation and growth. With 0.7 weight percent BPQDs assembled into CsPbI₂Br, X. Gong et al. achieved a record 15.5% PCE with FF of 78%.^[64] Due to lone-pair electrons in BPQDs, a strong binding was achieved between phosphorus and the Cs cations of CsPbI₂Br. This contributed to the stabilization of the α phase and the growth of a more uniform QDiP film. Carbon QDs have also been included in MAPbI₃ for solar cells:^[67] the carbonyl functional groups on the surface of carbon QDs slow perovskite growth and lead to the formation of large grains. The hydroxyl and carbonyl groups passivate the dangling lead ions and reduce nonradiative recombination. The fabricated device shows a maximum PCE of 18.24% with a FF of 78%.

QDiP have also been investigated as a promising choice for intermediate-solar cells (IBSC).^[68,69] H. Hosokawa et al. replaced MAPbI₃ with MAPbBr₃ and prepared PbS-MAPbBr₃ QDiP, suggesting avenues to QDiP in IBSC.^[70,71] IBSCs provide three photon absorption channels: from the VB to CB, from the intermediate band (IB) to CB, and from the VB to IB. For the PbS-MAPbBr₃ QDiP, MAPbBr₃ has a bandgap of 2.3 eV and PbS has a band gap of 1.0 eV. These values match closely those of the ideal IBSC, a bulk bandgap of 2.4 eV split into IBs of 1.5 and 0.9 eV.^[70] The authors confirmed IB formation, witnessing a blueshift in the PL spectrum. Though a low PCE of 1.9% was achieved to date, further studies may improve performance.

4.3. QDiP in Sensing and Beyond

Perovskite-based photodetectors have shown promise in EQE, leveraging their direct bandgap;^[72–74] though the dark current remains an area for improvement in these materials and devices. QDiP offer a route to extend responsivity into the infrared.^[75] Z. H. Duan et al. embedded CuInSe₂ CQDs into a MAPbI₃ matrix for broadband photodetectors.^[41] The CuInSe₂ CQDs are covered with oleylamine ligands, with the high-resistance ligands suppressing dark current. CuInSe₂

CQDs function as a sensitizer for light harvesting, while the MAPbI₃ component generates photocurrent. The photodetectors responded across the visible spectral range with an on/off ratio of 10⁴ at 2 V under 525 nm illumination. The photodetectors are stable for 7 days following extended air exposure, unencapsulated. Using PbS-MaPbI_{2.5}Br_{0.5} QDiP, F. P. G. Arquer et al. obtained QCD photodiodes in the short-wavelength infrared (SWIR) region.^[76] Their specific detectivities ($D^* \approx 4 \times 10^{12}$ Jones) in the SWIR outperform those of previous related reports more than twofold. The CQDs provide sensitization, and the perovskite matrix the transport medium.

Ionizing radiation detection demands a host material and activators as provided in QDiP. The matrix of the host is ideally formed using materials consisting of heavy elements (i.e., having high atomic numbers) so that the radiation energy is focused within the matrix. The energy needs to be quickly transferred to the activator. Superlattices of CsPbBr₃-Cs₄PbBr₆ match the material requirement for ionizing radiation detection. F. Cao et al. pursued the detection of ionizing radiation using the CsPbBr₃-Cs₄PbBr₆ QDiP,^[77,78] specifically for X-ray sensing and imaging. The Cs₄PbBr₆ matrix contributed to the attenuation of X-rays and stabilization of CsPbBr₃, while remaining transparent to green emission from CsPbBr₃. The authors obtained an impressively large-area film of 360 mm × 240 mm.

5. Conclusion and Perspective

In this progress report, we summarized the advances in QDiP since the time of early studies. For synthesis, surface modification of the CQDs using halide perovskite precursors enabled integration into a perovskite matrix. A compact interface controlled nucleation and growth of the perovskite enabled charge transfer from the matrix to CQDs or the transfer from CQDs to the matrix. QDiP offers encouraging properties and performance in LEDs, solar cells, photodetectors, field emission, and X-ray detectors.

Quantum-dot-in-perovskite solids unite the benefits of CQDs with those of halide perovskites. Only a few combinations of CQD and halide perovskite materials have been used to synthesize QDiP, leaving unexplored a large material space. Understanding further the optical and electrical properties of QDiP is still required. The impact of the size of CQDs, the crystal growth dynamics of the perovskite on the different CQD facets, and the band alignment at the interface all warrant further study. The potential of QDiP to solve the intrinsic instability problems of solution-based semiconductors calls for more attention to these material systems, and more detailed studies to understand the role of strain in the stability improvement of QDiP-based devices are required. The performance of QDiP in devices can not only be further improved but also extended to other applications. Current reports focus on LEDs and solar cells; while less-explored routes such as photodetectors (spanning from X-rays to mid-IR) also hold opportunities. The incorporation of CQDs into perovskites is of interest in applications where dipole-alignment is of use, such as electro-optics and piezoelectricity, due to the alignment provided by lattice-anchoring. Furthermore, QDiP with a type-I heterojunction may contribute to the threshold reduction of solution-based lasers. The excitonic

transport from the perovskite to the CQD leads to localized population inversion at lower excitation powers. Overall, QDiP is a strategy to enhance the performance of CQD-based optoelectronic devices, and to extend the diversity of perovskite-based materials.

Acknowledgements

This work was supported by the financial support from the Ontario Research Fund-Research Excellence Program and from the Natural Sciences and Engineering Research Council of Canada (NSERC).

Conflict of Interest

The authors declare no conflict of interest.

Keywords

hybrid materials, light-emitting diodes, quantum-dot-in-perovskite solids, solar-cells, solution-based

Received: March 6, 2021

Revised: April 18, 2021

Published online:

- [1] M. F. Ashby, Y. J. Bréchet, *Acta Mater.* **2003**, *51*, 5801.
- [2] Z. Ning, X. Gong, R. Comin, G. Walters, F. Fan, O. Voznyy, E. Yassitepe, A. Buin, S. Hoogland, E. H. Sargent, *Nature* **2015**, *523*, 324.
- [3] Q. L. He, H. Liu, M. He, Y. H. Lai, H. He, G. Wang, K. T. Law, R. Lortz, J. Wang, I. K. Sou, *Nat. Commun.* **2014**, *5*, 4247.
- [4] C. Jin, E. C. Regan, A. Yan, M. I. B. Utama, D. Wang, S. Zhao, Y. Qin, S. Yang, Z. Zheng, S. Shi, *Nature* **2019**, *567*, 76.
- [5] K. L. Seyler, P. Rivera, H. Yu, N. P. Wilson, E. L. Ray, D. G. Mandrus, J. Yan, W. Yao, X. Xu, *Nature* **2019**, *567*, 66.
- [6] M. Kalaj, K. C. Bentz, S. Ayala Jr., J. M. Palomba, K. S. Barcus, Y. Katayama, S. M. Cohen, *Chem. Rev.* **2020**, *120*, 8267.
- [7] T. Kitao, Y. Zhang, S. Kitagawa, B. Wang, T. Uemura, *Chem. Soc. Rev.* **2017**, *46*, 3108.
- [8] N. Tessler, V. Medvedev, M. Kazes, S. Kan, U. Banin, *Science* **2002**, *295*, 1506.
- [9] C. R. Kagan, E. Lifshitz, E. H. Sargent, D. V. Talapin, *Science* **2016**, *353*, aac5523.
- [10] E. H. Sargent, *Nat. Photonics* **2012**, *6*, 133.
- [11] K.-S. Cho, K. Heo, C.-W. Baik, J. Y. Choi, H. Jeong, S. Hwang, S. Y. Lee, *Nat. Commun.* **2017**, *8*, 840.
- [12] C. Livache, B. Martinez, N. Goubet, C. Gréboval, J. Qu, A. Chu, S. Royer, S. Ithurria, M. G. Silly, B. Dubertret, *Nat. Commun.* **2019**, *10*, 2125.
- [13] W. Zhou, Y. Shang, F. P. G. de Arquer, K. Xu, R. Wang, S. Luo, X. Xiao, X. Zhou, R. Huang, E. H. Sargent, *Nat. Electron.* **2020**, *3*, 251.
- [14] X. Li, Y.-B. Zhao, F. Fan, L. Levina, M. Liu, R. Quintero-Bermudez, X. Gong, L. N. Quan, J. Fan, Z. Yang, *Nat. Photonics* **2018**, *12*, 159.
- [15] X. Hou, J. Kang, H. Qin, X. Chen, J. Ma, J. Zhou, L. Chen, L. Wang, L.-W. Wang, X. Peng, *Nat. Commun.* **2019**, *10*, 1750.
- [16] S.-W. Baek, S. Jun, B. Kim, A. H. Proppe, O. Ouellette, O. Voznyy, C. Kim, J. Kim, G. Walters, J. H. Song, *Nat. Energy* **2019**, *4*, 969.
- [17] J. S. Manser, P. V. Kamat, *Nat. Photonics* **2014**, *8*, 737.
- [18] A. K. Jena, A. Kulkarni, T. Miyasaka, *Chem. Rev.* **2019**, *119*, 3036.
- [19] H. Dong, C. Zhang, X. Liu, J. Yao, Y. S. Zhao, *Chem. Soc. Rev.* **2020**, *49*, 951.
- [20] X. Li, J. M. Hoffman, M. G. Kanatzidis, *Chem. Rev.* **2021**, *121*, 2230.
- [21] X. Zhang, M. Lu, Y. Zhang, H. Wu, X. Shen, W. Zhang, W. Zheng, V. L. Colvin, W. W. Yu, *ACS Cent. Sci.* **2018**, *4*, 1352.
- [22] S. Wang, C. Bi, A. Portniagin, J. Yuan, J. Ning, X. Xiao, X. Zhang, Y. Y. Li, S. V. Kershaw, J. Tian, *ACS Energy Lett.* **2020**, *5*, 2401.
- [23] X. Xu, X. Wang, *Small Struct.* **2020**, *1*, 2000009.
- [24] Y. Chen, Y. Zhao, *J. Mater. Chem. A* **2020**, *8*, 25017.
- [25] D. M. Balazs, M. A. Loi, *Adv. Mater.* **2018**, *30*, 1800082.
- [26] R. J. Ellingson, M. C. Beard, J. C. Johnson, P. Yu, O. I. Micic, A. J. Nozik, A. Shabaev, A. L. Efros, *Nano Lett.* **2005**, *5*, 865.
- [27] J. E. Murphy, M. C. Beard, A. G. Norman, S. P. Ahrenkiel, J. C. Johnson, P. Yu, O. I. Micic, R. J. Ellingson, A. J. Nozik, *J. Am. Chem. Soc.* **2006**, *128*, 3241.
- [28] L.-W. Wang, A. Zunger, *Phys. Rev. B* **1996**, *53*, 9579.
- [29] Y. Li, Y. Ding, Y. Zhang, Y. Qian, *J. Phys. Chem. Solids* **1999**, *60*, 13.
- [30] A. Franceschetti, A. Zunger, *Phys. Rev. B* **2000**, *62*, 2614.
- [31] D. V. Talapin, J.-S. Lee, M. V. Kovalenko, E. V. Shevchenko, *Chem. Rev.* **2010**, *110*, 389.
- [32] L. Mao, C. C. Stoumpos, M. G. Kanatzidis, *J. Am. Chem. Soc.* **2018**, *141*, 1171.
- [33] Y. Liu, Z. Xu, Z. Yang, Y. Zhang, J. Cui, Y. He, H. Ye, K. Zhao, H. Sun, R. Lu, *Matter* **2020**, *3*, 180.
- [34] C. C. Stoumpos, M. G. Kanatzidis, *Adv. Mater.* **2016**, *28*, 5778.
- [35] L. N. Quan, R. Quintero-Bermudez, O. Voznyy, G. Walters, A. Jain, J. Z. Fan, X. Zheng, Z. Yang, E. H. Sargent, *Adv. Mater.* **2017**, *29*, 1605945.
- [36] C. Fan, X. Xu, K. Yang, F. Jiang, S. Wang, Q. Zhang, *Adv. Mater.* **2018**, *30*, 1804707.
- [37] M. A. Hines, G. D. Scholes, *Adv. Mater.* **2003**, *15*, 1844.
- [38] A. H. Ip, S. M. Thon, S. Hoogland, O. Voznyy, D. Zhitomirsky, R. Debnath, L. Levina, L. R. Rollny, G. H. Carey, A. Fischer, *Nat. Nanotechnol.* **2012**, *7*, 577.
- [39] Z. Yang, A. Janmohamed, X. Lan, F. P. García de Arquer, O. Voznyy, E. Yassitepe, G.-H. Kim, Z. Ning, X. Gong, R. Comin, *Nano Lett.* **2015**, *15*, 7539.
- [40] J. Han, X. Yin, H. Nan, Y. Zhou, Z. Yao, J. Li, D. Oron, H. Lin, *Small* **2017**, *13*, 1700953.
- [41] Z. Duan, J. Ning, M. Chen, Y. Xiong, W. Yang, F. Xiao, S. V. Kershaw, N. Zhao, S. Xiao, A. L. Rogach, *ACS Appl. Mater. Interfaces* **2020**, *12*, 35201.
- [42] T. W. Kim, S. Uchida, T. Matsushita, L. Cojocar, R. Jono, K. Kimura, D. Matsubara, M. Shirai, K. Ito, H. Matsumoto, *Adv. Mater.* **2018**, *30*, 1705230.
- [43] M. Sytnyk, S. Yakunin, W. Schöfberger, R. T. Lechner, M. Burian, L. Ludescher, N. A. Killilea, A. YousefiAmin, D. Kriegner, J. Stangl, *ACS Nano* **2017**, *11*, 1246.
- [44] L. Gao, L. N. Quan, F. P. G. de Arquer, Y. Zhao, R. Munir, A. Proppe, R. Quintero-Bermudez, C. Zou, Z. Yang, M. I. Saidaminov, *Nat. Photonics* **2020**, *14*, 227.
- [45] A. Younis, L. Hu, P. Sharma, C. H. Lin, Y. Mi, X. Guan, D. Zhang, Y. Wang, T. He, X. Liu, *Adv. Funct. Mater.* **2020**, *30*, 2002948.
- [46] S. Masi, C. Echeverría-Arrondo, K. M. Salim, T. T. Ngo, P. F. Mendez, E. López-Fraguas, D. F. Macías-Pinilla, J. Planellas, J. I. Climente, I. Mora-Sero, *ACS Energy Lett.* **2020**, *5*, 418.
- [47] M. Liu, Y. Chen, C.-S. Tan, R. Quintero-Bermudez, A. H. Proppe, R. Munir, H. Tan, O. Voznyy, B. Scheffel, G. Walters, *Nature* **2019**, *570*, 96.
- [48] Q. Jiang, Y. Zhao, X. Zhang, X. Yang, Y. Chen, Z. Chu, Q. Ye, X. Li, Z. Yin, J. You, *Nat. Photonics* **2019**, *13*, 460.
- [49] D. P. McMeekin, G. Sadoughi, W. Rehman, G. E. Eperon, M. Saliba, M. T. Hörantner, A. Haghighirad, N. Sakai, L. Korte, B. Rech, *Science* **2016**, *351*, 151.

- [50] D. Yao, C. Zhang, N. D. Pham, Y. Zhang, V. T. Tiong, A. Du, Q. Shen, G. J. Wilson, H. Wang, *J. Phys. Chem. Lett.* **2018**, *9*, 2113.
- [51] M. Saliba, T. Matsui, K. Domanski, J.-Y. Seo, A. Ummadisingu, S. M. Zakeeruddin, J.-P. Correa-Baena, W. R. Tress, A. Abate, A. Hagfeldt, *Science* **2016**, *354*, 206.
- [52] Z.-Z. Luo, S. Hao, S. Cai, T. P. Bailey, G. Tan, Y. Luo, I. Spanopoulos, C. Uher, C. Wolverton, V. P. Dravid, *J. Am. Chem. Soc.* **2019**, *141*, 6403.
- [53] X. Gong, Z. Yang, G. Walters, R. Comin, Z. Ning, E. Beauregard, V. Adinolfi, O. Voznyy, E. H. Sargent, *Nat. Photonics* **2016**, *10*, 253.
- [54] X. Zhang, X. Wu, X. Liu, G. Chen, Y. Wang, J. Bao, X. Xu, X. Liu, Q. Zhang, K. Yu, *J. Am. Chem. Soc.* **2020**, *142*, 4464.
- [55] J. S. Steckel, S. Coe-Sullivan, V. Bulović, M. G. Bawendi, *Adv. Mater.* **2003**, *15*, 1862.
- [56] Z. Yang, O. Voznyy, G. Walters, J. Z. Fan, M. Liu, S. Kinge, S. Hoogland, E. H. Sargent, *ACS Photonics* **2017**, *4*, 830.
- [57] M. Vasilopoulou, H. P. Kim, B. S. Kim, M. Papadakis, A. E. X. Gavim, A. G. Macedo, W. J. da Silva, F. K. Schneider, M. A. M. Teridi, A. G. Coutsolelos, *Nat. Photonics* **2020**, *14*, 50.
- [58] V. Sukhovatkin, S. Hinds, L. Brzozowski, E. H. Sargent, *Science* **2009**, *324*, 1542.
- [59] L. Etgar, P. Gao, P. Qin, M. Graetzel, M. K. Nazeeruddin, *J. Mater. Chem. A* **2014**, *2*, 11586.
- [60] X. Zhang, J. Zhang, D. Phuyal, J. Du, L. Tian, V. A. Öberg, M. B. Johansson, U. B. Cappel, O. Karis, J. Liu, *Adv. Energy Mater.* **2018**, *8*, 1702049.
- [61] J. Peng, Y. Chen, X. Zhang, A. Dong, Z. Liang, *Adv. Sci.* **2016**, *3*, 1500432.
- [62] Y. Wang, S. Liu, B. Zeng, H. Huang, J. Xiao, J. Li, M. Long, S. Xiao, X. Yu, Y. Gao, *Nanoscale* **2017**, *9*, 4683.
- [63] R. Long, W. Fang, A. V. Akimov, *J. Phys. Chem. Lett.* **2016**, *7*, 653.
- [64] X. Gong, L. Guan, Q. Li, Y. Li, T. Zhang, H. Pan, Q. Sun, Y. Shen, C. Grätzel, S. M. Zakeeruddin, *Sci. Adv.* **2020**, *6*, eaay5661.
- [65] W. Yang, J. Chen, X. Lian, J. Li, F. Yao, G. Wu, W. Qiu, C. Jin, P. Heremans, H. Chen, *Sol. RRL* **2019**, *3*, 1900132.
- [66] Y. Wang, H. Zhang, T. Zhang, W. Shi, M. Kan, J. Chen, Y. Zhao, *Sol. RRL* **2019**, *3*, 1900197.
- [67] Y. Ma, H. Zhang, Y. Zhang, R. Hu, M. Jiang, R. Zhang, H. Lv, J. Tian, L. Chu, J. Zhang, *ACS Appl. Mater. Interfaces* **2018**, *11*, 3044.
- [68] A. Martí, E. Antolín, C. Stanley, C. Farmer, N. López, P. Díaz, E. Cánovas, P. Linares, A. Luque, *Phys. Rev. Lett.* **2006**, *97*, 247701.
- [69] E. López, A. Datas, I. Ramiro, P. Linares, E. Antolín, I. Artacho, A. Martí, A. Luque, Y. Shoji, T. Sogabe, *Sol. Energy Mater. Sol. Cells* **2016**, *149*, 15.
- [70] H. Hosokawa, R. Tamaki, T. Sawada, A. Okonogi, H. Sato, Y. Ogomi, S. Hayase, Y. Okada, T. Yano, *Nat. Commun.* **2019**, *10*, 43.
- [71] I. Ramiro, A. Martí, *Prog. Photovolt. Res. Appl.* **2020**, *1*.
- [72] L. Dou, Y. M. Yang, J. You, Z. Hong, W.-H. Chang, G. Li, Y. Yang, *Nat. Commun.* **2014**, *5*, 5404.
- [73] X. Hu, X. Zhang, L. Liang, J. Bao, S. Li, W. Yang, Y. Xie, *Adv. Funct. Mater.* **2014**, *24*, 7373.
- [74] H. L. Zhu, J. Cheng, D. Zhang, C. Liang, C. J. Reckmeier, H. Huang, A. L. Rogach, W. C. Choy, *ACS Nano* **2016**, *10*, 6808.
- [75] C. Liu, H. Peng, K. Wang, C. Wei, Z. Wang, X. Gong, *Nano Energy* **2016**, *30*, 27.
- [76] F. P. G. de Arquer, X. Gong, R. P. Sabatini, M. Liu, G.-H. Kim, B. R. Sutherland, O. Voznyy, J. Xu, Y. Pang, S. Hoogland, D. Sinton, E. Sargent, *Nat. Commun.* **2017**, *8*, 14757.
- [77] R. T. Williams, W. W. Wolszczak, X. Yan, D. L. Carroll, *ACS Nano* **2020**, *14*, 5161.
- [78] F. Cao, D. Yu, W. Ma, X. Xu, B. Cai, Y. M. Yang, S. Liu, L. He, Y. Ke, S. Lan, *ACS Nano* **2019**, *14*, 5183.



Haijie Chen received his Ph.D. (2014) from Shanghai Institute of Ceramics, Chinese Academy of Sciences, China. From 2015 to 2019, he held a postdoctoral appointment at Northwestern University with Prof. Mercouri G. Kanatzidis. Since 2019, he has been working with Prof. Edward H. Sargent at the University of Toronto as a postdoctoral fellow. His research focuses on the exploration of new chalcogenide and halide materials and their optoelectrical applications. Now he is a researcher at Donghua University.



Joao M. Pina received his M.Sc. degree (2018) in Nanotechnology from the KTH Royal Institute of Technology, Stockholm. He is currently pursuing his Ph.D. degree under the supervision of Prof. Edward H. Sargent at the University of Toronto. His recent research interests focus on the development of next-generation IR materials for optoelectronic applications.



Yi Hou completed his Ph.D. in 2017 at the University of Erlangen-Nuremberg in Germany and joined the Clarendon Laboratory Department of Physics at the University of Oxford as a visiting Ph.D. student. After the completion of his doctoral degree, he first moved to the University of Toronto (2018–2020) in Canada, where he worked as a postdoctoral fellow focusing on the understanding of photophysics and transport properties in perovskite/Si tandem solar cell. Now he is an assistant professor at the National University of Singapore.



Edward H. Sargent is the university professor in the Edward S. Rogers Sr. Department of Electrical and Computer Engineering at the University of Toronto. He holds the Canada Research Chair in Nanotechnology and also serves as Vice President–Research for the University of Toronto.